Radiative QED corrections to one-photon transition rates in the hydrogen atom at finite temperatures

T. Zalialiutdinov,[1] D. Solovyev,[1] and L. Labzowsky[1,2]
[1]*Department of Physics, St. Petersburg State University, Petrodvorets, Oulianovskaya 1, 198504 St. Petersburg, Russia*
[2]*Petersburg Nuclear Physics Institute, 188300 Gatchina, St. Petersburg, Russia*

(Received 8 February 2020; accepted 15 April 2020; published 8 May 2020)

Within the framework of QED theory at finite temperature, the thermal radiative corrections to spontaneous one-photon transition rates in hydrogen atom are investigated. The radiative one-loop self-energy corrections are described in the thermal case. Closed analytical expressions are derived and their numerical calculations for the spontaneous decay rate of the $2p$ state are carried out. The dominance of thermal radiative corrections to a spontaneous Ly_α decay rate over an ordinary induced transition rate up to temperatures $T < 6000$ K is demonstrated.

DOI: 10.1103/PhysRevA.101.052503

I. INTRODUCTION

Radiative corrections to transition rates and lifetimes in atoms and ions are of no less interest than radiative corrections to the energies of bound states (such as corrections to the Lamb shift, hyperfine splitting, etc.) [1–4]. The precision in measurements of decay rates has considerably increased in recent years, which has been accompanied by a corresponding increase in the accuracy of theoretical calculations [5–11]. The experimental uncertainty achieved at the level of one per thousand [12] makes such studies sensitive to relativistic, radiative, nuclear size, and recoil effects [4,13–17]. Therefore, the detailed theoretical analysis of various radiative corrections providing a versatile verification of fundamental physics is required. The precise values of the transition rates in different atomic systems are also needed for investigations of atomic collision processes or interpretation of the spectra from astrophysical sources [18]. Moreover, accurate calculations of the transition rates can serve for verifications of basic parts in more complicated processes, such as the parity violation amplitudes in heavy ions and atoms [19,20]. In this regard, radiative corrections to the transition rates become extremely important for the decay rates suppressed with respect to dipole transitions (forbidden by selection rules) [1,16]. To date, theoretical calculations of such decay rates have advanced to the evaluation of the two-loop self-energy diagrams [3,21,22].

The accounting of different radiative effects required to achieve the experimental uncertainty draws attention to other types of phenomena. The impact of physical conditions, such as external fields for example, on laboratory experiment and astrophysical processes deserves special consideration [23–27]. As a separate area of research, the influence of blackbody radiation (BBR) at finite temperatures plays an important role in a number of scenarios: development of atomic clocks, recombination history of the early universe, or radiation transfer in an interstellar medium [28–34]. The quantum mechanical (QM) theory of energy shift and transition rates induced by the BBR is given in [35]. Theoretical calculations within the framework of rigorous quantum electrodynamics (QED) of the thermal Stark shift, level broadening, and BBR-induced bound-free transitions have been carried out in [37], and later in [38–40]. The advantage of QED theory application to investigations of this kind is the accurate accounting for finite lifetimes of atomic levels. Although such effects are outside the scope of this work, the formalism developed in [37–40] (see, also, [36]) can reveal new (unknown) thermal corrections to transition rates between bound states and analyze their significance at astrophysical and laboratory conditions.

In the present work, the radiative one-loop self-energy (SE) corrections caused by the "heat bath" to the one-photon transition rates for the hydrogen atom are investigated within the framework of thermal QED theory. The heat bath acting on the atomic system implies an environment described by blackbody radiation, i.e., the photon field distributed according to Planck's law. We restrict ourselves to considering the leading SE thermal corrections to the transition rates, since the next orders or effects associated with vacuum polarization (VP) are suppressed by temperature factors and, therefore, should be much less [1,4,36].

The paper is organized as follows. In Sec. II, we briefly describe the adiabatic S-matrix approach for the evaluation of one-photon transition probabilities in one-electron atomic systems. The derivation of SE thermal radiative corrections is considered in Sec. III. Expressions derived in Sec. III are applied to the numerical calculation of thermal corrections to the $2p \to 1s + \gamma(\mathrm{E1})$ transition rate in hydrogen. The results of the calculations are discussed in Sec. IV. Below we will use the relativistic units $\hbar = m_e = c = 1$ (m_e is the electron rest mass, c is the speed of light, and $\hbar$ is the reduced Planck constant).

II. ADIABATIC S-MATRIX APPROACH: EVALUATION OF TRANSITION RATE

For evaluation of the transition probabilities and radiative corrections, we will use the adiabatic S-matrix approach

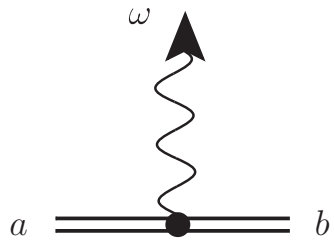

FIG. 1. The Feynman graph corresponding to the photon emission in a one-electron atom. The double solid line describes the electron in the field of a nucleus (Furry picture); the wavy line with the arrow at the end describes the emitted photon. The indices a and b refer to the set of quantum numbers of the initial and final states of an atom, respectively; ω denotes the frequency of the emitted photon.

[41–43]. This allows one to take into account contributions to QED corrections arising from the reducible Feynman diagrams [24,44]. The adiabatic S_η matrix differs from the ordinary S matrix by the insertion of the exponential factor $e^{-\eta|t|}$ ($\eta > 0$ is the adiabatic parameter) in each vertex of the Feynman diagram. It refers to the concept of adiabatic switching on and off of the interaction formally introduced by the replacement, $\hat{H}_{\rm int}(t) \to \hat{H}^{\eta}_{\rm int}(t) = e^{-\eta|t|}\hat{H}_{\rm int}(t)$ [2,3].

For the one-electron atom, the one-photon transition from state a to state b is described by the Feynman diagram in Fig. 1. Within the framework of the adiabatic S-matrix approach, the corresponding first-order S-matrix element is

$$\hat{S}^{(1)}_{ab} = (-ie)\int dx\overline{\psi}_b(x)\gamma_\mu A^*_\mu(x)e^{-\eta|t|}\psi_a(x). \tag{1}$$

Here, e is the electron charge, $\psi_a(x) = \psi_a(\mathbf{r})e^{-iE_at}$ is the solution of Dirac's equation for the atomic electron, E_a is the Dirac energy of state a, $\overline{\psi}_a = \psi^\dagger_a\gamma_0$ is the Dirac conjugated wave function with $\psi^\dagger_a$ being its Hermitian conjugate, and $\gamma_\mu = (\gamma_0, \boldsymbol{\gamma})$ are the Dirac matrices. Photon field wave function $A^{(\mathbf{k},\mathbf{e})}_\mu(x)$ is

$$A^{(\mathbf{k},\mathbf{e})}_\mu(x) = \sqrt{\frac{2\pi}{\omega}}e^{(\lambda)}_\mu e^{i(\mathbf{kr}-\omega t)} = \sqrt{\frac{2\pi}{\omega}}e^{(\lambda)}_\mu e^{-i\omega t}A^{(\mathbf{k},\mathbf{e})}_\mu(\mathbf{r}), \tag{2}$$

where $e^{(\lambda)}_\mu$ is the polarization 4-vector, $\mathbf{k}$ is the wave vector, $\omega = |\mathbf{k}|$ is the photon frequency, and $x \equiv (\mathbf{r}, t)$ is the coordinate 4-vector, where ($\mathbf{r}$, t are the space and time coordinates).

Following the standard evaluation of S-matrix theory, the transition rate is [42,43]

$$W_{ab} = \lim_{\eta\to 0+}\eta\sum_{\mathbf{e}}\int\left|\hat{S}^{(1)}_{ab}\right|^2\frac{d\mathbf{k}}{(2\pi)^3}, \tag{3}$$

where $d\mathbf{k} = \omega^2 d\omega d\boldsymbol{\nu}$ and $\boldsymbol{\nu} = \mathbf{k}/|\mathbf{k}|$ is the photon propagation vector. The integration over the time variable in Eq. (1) essentially yields a representation of the δ function [43,45],

$$\int_{-\infty}^{\infty} dt e^{i(E_b-E_a+\omega)t-\eta|t|} = \frac{2\eta}{(\omega_{ab}-\omega)^2+\eta^2} \equiv 2\pi\delta_\eta(\omega_{ab}-\omega). \tag{4}$$

Here, $\omega_{ab} = E_a - E_b$ and $\lim_{\eta\to 0+}\delta_\eta(x) = \delta(x)$. Then, taking Eq. (1) by square modulus and integrating over ω, one can arrive at

$$W_{ab} = \frac{\omega^2_{ab}}{(2\pi)^2}\sum_{\mathbf{e}}\int\left|\hat{U}^{(1)}_{ab}\right|^2 d\boldsymbol{\nu}, \tag{5}$$

where

$$\hat{U}^{(1)}_{ab} = (-ie)\sqrt{\frac{2\pi}{\omega_{ab}}}\langle b|(\mathbf{e}^*\boldsymbol{\alpha})e^{-i\mathbf{kr}}|a\rangle. \tag{6}$$

To obtain Eq. (5), the following relation was used [43,45]:

$$4\eta^2\int_{-\infty}^{+\infty}\frac{\omega d\omega}{[(\omega_{ab}-\omega)^2+\eta^2]^2} = \frac{2\pi\omega_{ab}}{\eta}. \tag{7}$$

In the nonrelativistic limit, $\mathbf{kr} \sim \alpha Z \ll 1$, the use of the dipole approximation for the transition amplitude (6) leads to

$$\hat{U}^{(1)}_{ab} = (-ie)\sqrt{\frac{2\pi}{\omega_{ab}}}\langle b|\mathbf{e}^*\mathbf{p}|a\rangle, \tag{8}$$

where $\langle a|\hat{T}|b\rangle$ now denotes the matrix element of operator $\hat{T}$ with Schrödinger wave functions for an atomic electron in the Coulomb field. Substituting Eq. (8) into Eq. (5), performing summation over photon polarizations, and integration over photon directions, one can arrive at

$$W_{ab} = \frac{4e^2}{3}\omega_{ab}|\langle b|\mathbf{p}|a\rangle|^2. \tag{9}$$

Finally, the summation over the magnetic quantum numbers of the final state and averaging over magnetic quantum numbers of the initial state in Eq. (9) should be performed. Then, employing the quantum mechanical relation

$$\langle a|\mathbf{p}|b\rangle = i\omega_{ab}\langle a|\mathbf{r}|b\rangle, \tag{10}$$

the partial transition rate corresponding to the emission process $a \to b + \gamma$(E1) is given by the expression

$$W_{ab} = \frac{4e^2}{3}\frac{1}{2l_a+1}\sum_{m_am_b}\omega^3_{ab}|\langle b|\mathbf{r}|a\rangle|^2. \tag{11}$$

In the presence of the BBR field, i.e., isotropic external radiation field with equilibrium temperature T, the partial induced transition can be additionally found in the form

$$W^{\rm ind}_{ab} = \frac{4e^2}{3}\frac{1}{2l_a+1}\sum_{m_am_b}\omega^3_{ab}|\langle b|\mathbf{r}|a\rangle|^2 n_\beta(\omega_{ab}), \tag{12}$$

where $n_\beta(\omega)$ is the Planck distribution function $n_\beta(\omega) = (e^{\beta\omega}-1)^{-1}$, $\beta \equiv 1/k_BT$, and k_B is the Boltzmann constant. The thermal background leads to the level broadening due to the BBR-induced transition to all possible final states. This broadening is represented by the sum over all final states (including continuum) [35],

$$\Gamma^{\rm BBR}_a = \frac{4e^2}{3}\frac{1}{2l_a+1}\sum_b\sum_{m_am_b}\omega^3_{ab}|\langle b|\mathbf{r}|a\rangle|^2 n_\beta(\omega_{ab}). \tag{13}$$

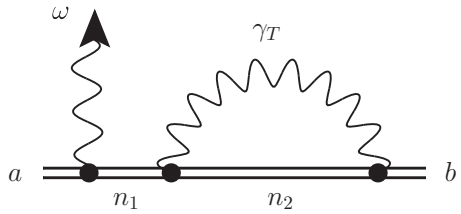

FIG. 2. The Feynman graph corresponding to the thermal one-loop QED correction to photon emission in a one-electron atom. The double solid line describes the electron in the field of the nucleus (Furry picture); the wavy line with the arrow at the end describes the emitted photon with frequency ω. The wavy line with index γ_T denotes the thermal photon propagator. The indices a and b refer to the quantum numbers of the initial and final states of an atom, respectively, while indices n_1 and n_2 refer to the quantum numbers of the intermediate states in electron propagators.

Then the total widths of level a is

$$\Gamma_a = \sum_{b<a} W_{ab} + \sum_b W^{\rm ind}_{ab} \equiv \Gamma^{\rm nat}_a + \Gamma^{\rm BBR}_a, \tag{14}$$

where $\Gamma^{\rm nat}_a$ is the natural width of level a. In the laboratory experiments, $\Gamma^{\rm BBR}_a$ is actually small for the low-lying atomic levels, but becomes important for the Rydberg states and increases with the growth of temperature. The induced transition rates with necessity are taken into account in the astrophysical investigations at high temperatures [33].

III. THERMAL SELF-ENERGY CORRECTIONS TO ONE-PHOTON TRANSITION RATE

The thermal (one-loop) self-energy corrections to the one-photon transition rate are given by the set of Feynman diagrams represented in Figs. 2–4. Then the one-photon transition probability corrected according to Figs. 2–4 is defined by

$$\widetilde{W}_{ab} = \lim_{\eta\to 0+} \eta \sum_{\mathbf{e}} \int \left|\hat{S}^{(1)}_{ab} + \hat{S}^{(3)}_{ab}\right|^2 \frac{d\mathbf{k}}{(2\pi)^3}, \tag{15}$$

where $\hat{S}^{(3)}_{ab}$ is the sum of three third-order S-matrix elements corresponding to the Feynman diagrams in Figs. 2 and 3. Taking the square modulus in Eq. (15) and neglecting by the terms proportional to e^6, the corrected transition rate takes the

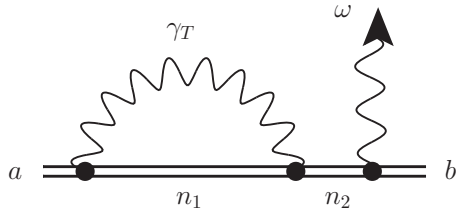

FIG. 3. The Feynman graph corresponding to the thermal one-loop QED correction to photon emission in a one-electron atom. All notations are the same as in Fig. 2.

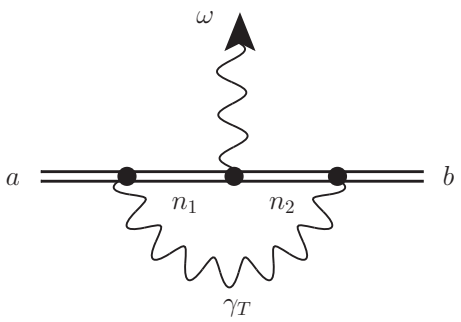

FIG. 4. The Feynman graph corresponding to the thermal one-loop QED correction to photon emission in a one-electron atom. All notations are the same as in Fig. 2.

form

$$\widetilde{W}_{ab} = \lim_{\eta\to 0+} \eta \sum_{\mathbf{e}} \int \left[\left|\hat{S}^{(1)}_{ab}\right|^2 + 2{\rm Re}\left(\hat{S}^{(1)*}_{ab} \times \hat{S}^{(3)}_{ab}\right)\right] \frac{d\mathbf{k}}{(2\pi)^3}, \tag{16}$$

where the first term in brackets in Eq. (16) leads to the expression (5) and the second term represents the thermal corrections.

We start from the evaluation of the thermal loop correction to a one-photon transition rate given by Fig. 2. The corresponding adiabatic S-matrix element is

$$\begin{aligned}\hat{S}^{(3){\rm Fig.2}}_{ab} = (-ie)^3 \int dx_3 dx_2 dx_1 \overline{\psi}_b(x_3) S(x_3, x_2) e^{-\eta|t_3|} \gamma_{\mu_3} \\ \times D^{\beta}_{\mu_3\mu_2}(x_3, x_2) e^{-\eta|t_2|} \gamma_{\mu_2} S(x_2, x_1) \gamma_{\mu_1} e^{-\eta|t_1|} \\ \times A^*_{\mu_1}(x_1) \psi_a(x_1),\end{aligned} \tag{17}$$

where $S(x_2x_1)$ is the Feynman propagator for the atomic electron and $D^{\beta}_{\mu\nu}(x_2, x_1)$ is the thermal photon propagator. In the Furry picture, the eigenmode's decomposition of the electron propagator reads [46]

$$S(x_2, x_1) = \frac{1}{2\pi i} \int_{-\infty}^{\infty} d\Omega\, e^{i\Omega(t_2-t_1)} \sum_n \frac{\psi_n(\mathbf{r}_2)\overline{\psi}_n(\mathbf{r}_1)}{E_n(1-i0)+\Omega}. \tag{18}$$

The summation in Eq. (18) extends over the entire Dirac spectrum of electron states n in the field of the nucleus. The thermal photon propagator $D^{\beta}_{\mu\nu}(x_2, x_1)$ in the Feynman gauge can be written in the form [36,37]

$$\begin{aligned} &D^{\beta}_{\mu\nu}(x_2, x_1) \\ &= -\frac{g_{\mu\nu}}{\pi r_{12}} \int_{-\infty}^{\infty} n_\beta(|\omega_\beta|) \sin(|\omega_\beta| {\rm r}_{12}) e^{-i\omega_\beta(t_2-t_1)} d\omega_\beta, \end{aligned} \tag{19}$$

where $r_{12} = |\mathbf{r}_1 - \mathbf{r}_2|$ and $g_{\mu\nu}$ is the metric tensor.

Integration over the time variables in Eq. (17) yields

$$\hat{S}_{ab}^{(3)\text{Fig.2}} = \frac{(-ie)^3}{4\pi^3}\int_{-\infty}^{\infty} d\Omega_1 \int_{-\infty}^{\infty} d\Omega_2 \frac{8\eta^3}{[(E_a+\Omega_2-\omega)^2+\eta^2][(\Omega_2-\Omega_1+\omega_\beta)^2+\eta^2][(E_b+\Omega_1-\omega_\beta)^2+\eta^2]}$$
$$\times\sqrt{\frac{2\pi}{\omega}}\int_{-\infty}^{\infty} d\omega_\beta n_\beta(|\omega_\beta|)\sum_{n_2 n_1}\frac{\langle n_1|(\mathbf{e}^*\boldsymbol{\alpha})e^{-i\mathbf{kr}}|a\rangle}{E_{n_1}(1-i0)+\Omega_2}\frac{\langle bn_2|\frac{1-\boldsymbol{\alpha}_2\boldsymbol{\alpha}_3}{r_{23}}\sin(|\omega_\beta|r_{23})|n_2 n_1\rangle}{E_{n_2}(1-i0)+\Omega_1}, \tag{20}$$

where integration over variables Ω_1 and Ω_2 in Eq. (20) can be performed with the use of the Cauchy theorem. The result is

$$\int_{-\infty}^{\infty} d\Omega_1 \int_{-\infty}^{\infty} d\Omega_2 \frac{8\eta^3}{[(E_a+\Omega_2-\omega)^2+\eta^2][(\Omega_2-\Omega_1+\omega_\beta)^2+\eta^2][(E_b+\Omega_1-\omega_\beta)^2+\eta^2]}$$
$$\times\frac{1}{E_{n_1}(1-i0)+\Omega_2}\frac{1}{E_{n_2}(1-i0)+\Omega_1} = \frac{1}{\omega_{n_1 b}-2i\eta}\frac{1}{\omega_{n_2 b}+\omega_\beta-i\eta-i0}\frac{24\pi^2\eta}{(\omega_{ab}-\omega)^2+(3\eta)^2}. \tag{21}$$

Following definition (16), the correction to the one-photon transition rate can be found as

$$\Delta W_{ab} = \lim_{\eta\to 0+}\eta\sum_{\mathbf{e}}\int 2\text{Re}\big(\hat{S}_{ab}^{(1)*}\times\hat{S}_{ab}^{(3)}\big)\frac{\omega^2 d\omega d\boldsymbol{v}}{(2\pi)^3}. \tag{22}$$

Taking in mind that Eq. (21) is multiplied by expression (4), the integration over photon frequency ω should be performed,

$$\int_{-\infty}^{+\infty}\frac{2\eta}{(\omega_{ab}-\omega)^2+\eta^2}\frac{24\pi^2\eta}{(\omega_{ab}-\omega)^2+(3\eta)^2}\omega d\omega = \frac{4\pi^3\omega_{ab}}{\eta}. \tag{23}$$

Then, Eq. (22) reduces to

$$\Delta W_{ab} = \text{Re}\left(\omega_{ab}^2\sum_{\mathbf{e}}\int\hat{U}_{ab}^{(1)*}\hat{U}_{ab}^{(3)}d\boldsymbol{v}\right), \tag{24}$$

where

$$\hat{U}_{ab}^{(3)\text{Fig.2}} = \frac{(-ie)^3}{4\pi^3}\sqrt{\frac{2\pi}{\omega_{ab}}}\int_{-\infty}^{\infty} d\omega_\beta n_\beta(|\omega_\beta|)\sum_{n_2 n_1}\frac{\langle n_1|(\mathbf{e}^*\boldsymbol{\alpha})e^{-i\mathbf{kr}}|a\rangle}{\omega_{n_1 b}-2i\eta}\frac{\langle bn_2|\frac{1-\boldsymbol{\alpha}_2\boldsymbol{\alpha}_3}{r_{23}}\sin(|\omega_\beta|r_{23})|n_2 n_1\rangle}{\omega_{n_2 b}+\omega_\beta-i\eta}$$
$$= \frac{(-ie)^3}{4\pi^3}\sqrt{\frac{2\pi}{\omega_{ab}}}\int_0^{\infty} d\omega_\beta n_\beta(\omega_\beta)\sum_{n_2 n_1}\frac{\langle n_1|(\mathbf{e}^*\boldsymbol{\alpha})e^{-i\mathbf{kr}}|a\rangle\langle bn_2|\frac{1-\boldsymbol{\alpha}_2\boldsymbol{\alpha}_3}{r_{23}}\sin(\omega_\beta r_{23})|n_2 n_1\rangle}{\omega_{n_1 b}-2i\eta}$$
$$\times\left(\frac{1}{\omega_{n_2 b}+\omega_\beta-i\eta}+\frac{1}{\omega_{n_2 b}-\omega_\beta-i\eta}\right). \tag{25}$$

The diagram shown in Fig. 2 and the corresponding amplitude given by Eq. (25) have a reducible part (reference state contribution) when $n_1 = b$. To evaluate it, we set $n_1 = b$ in Eq. (25) and consider the Taylor expansion in the vicinity of $\eta = 0$, which gives

$$\hat{U}_{ab(n_1=b)}^{(3)\text{Fig.2}} = \frac{(-ie)^3}{4\pi^3}\sqrt{\frac{2\pi}{\omega_{ab}}}\int_0^{\infty} d\omega_\beta n_\beta(\omega_\beta)\sum_{n_2}\langle b|(\mathbf{e}^*\boldsymbol{\alpha})e^{-i\mathbf{kr}}|a\rangle\langle bn_2|\frac{1-\boldsymbol{\alpha}_2\boldsymbol{\alpha}_3}{r_{23}}\sin(\omega r_{23})|n_2 b\rangle$$
$$\times\left\{\frac{i}{2\eta}\left(\frac{1}{\omega_{n_2 b}+\omega_\beta-i\eta}+\frac{1}{\omega_{n_2 b}-\omega_\beta-i\eta}\right)-\frac{1}{2}\left[\frac{1}{(\omega_{n_2 b}+\omega_\beta-i\eta)^2}+\frac{1}{(\omega_{n_2 b}-\omega_\beta-i\eta)^2}\right]+O(\eta)\right\}. \tag{26}$$

The real part [see Eq. (24)] of the first term in curly brackets in Eq. (26) multiplied by expression (8) vanishes with the accounting of the pure imaginary factor $1/(-2i\eta)$. Then, the combination of the reducible and irreducible contributions is

$$\hat{U}_{ab}^{(3)\text{Fig.2}} = \frac{(-ie)^3}{4\pi^3}\sqrt{\frac{2\pi}{\omega_{ab}}}\int_0^{\infty} d\omega_\beta n_\beta(\omega_\beta)\left\{\sum_{n_2,n_1\neq b}\frac{\langle n_1|(\mathbf{e}^*\boldsymbol{\alpha})e^{-i\mathbf{kr}}|a\rangle\langle bn_2|\frac{1-\boldsymbol{\alpha}_2\boldsymbol{\alpha}_3}{r_{23}}\sin(\omega_\beta r_{23})|n_2 n_1\rangle}{\omega_{n_1 b}}\right.$$
$$\times\left(\frac{1}{\omega_{n_2 b}+\omega_\beta-i\eta}+\frac{1}{\omega_{n_2 b}-\omega_\beta-i\eta}\right)-\frac{1}{2}\sum_{n_2}\langle b|(\mathbf{e}^*\boldsymbol{\alpha})e^{-i\mathbf{kr}}|a\rangle\langle bn_2|\frac{1-\boldsymbol{\alpha}_2\boldsymbol{\alpha}_3}{r_{23}}\sin(\omega_\beta r_{23})|n_2 b\rangle$$
$$\left.\times\left[\frac{1}{(\omega_{n_2 b}+\omega_\beta-i\eta)^2}+\frac{1}{(\omega_{n_2 b}-\omega_\beta-i\eta)^2}\right]\right\}. \tag{27}$$

One can note that the thermal corrections are suppressed by the factor of temperature in addition to the $Z\alpha$ expansion. Therefore, applying the nonrelativistic limits to the expression (27) can serve as an adequate approximation for the search for the dominant contribution. Within the dipole approximation $\mathbf{kr} \ll 1$, we have

$$\langle n_1|(\mathbf{e}^*\boldsymbol{\alpha})e^{-i\mathbf{kr}}|a\rangle = \langle n_1|\mathbf{e}^*\mathbf{p}|a\rangle = -i\omega_{an_1}\langle n_1|\mathbf{e}^*\mathbf{r}|a\rangle, \tag{28}$$

$$\begin{aligned}\langle bn_2|\frac{1-\boldsymbol{\alpha}_2\boldsymbol{\alpha}_3}{r_{23}}\sin(\omega_\beta r_{23})|n_2n_1\rangle &\approx \omega_\beta\langle b|n_2\rangle\langle n_2|n_1\rangle - \omega_\beta\langle b|\mathbf{p}|n_2\rangle\langle n_2|\mathbf{p}|n_1\rangle + \frac{\omega_\beta^3}{3}\langle b|\mathbf{r}|n_2\rangle\langle n_2|\mathbf{r}|n_1\rangle \\ &= \omega\langle b|n_2\rangle\langle n_2|n_1\rangle + \left(-\omega\omega_{n_2n_1}\omega_{n_2b} + \frac{\omega^3}{3}\right)\langle b|\mathbf{r}|n_2\rangle\langle n_2|\mathbf{r}|n_1\rangle,\end{aligned} \tag{29}$$

where the relation given by Eq. (10) was used. Then, substituting Eqs. (28) and (29) into Eq. (27), we find

$$\begin{aligned}\hat{U}_{ab}^{(3)\text{Fig.2}} = \frac{(-ie)^3}{4\pi^3}\sqrt{\frac{2\pi}{\omega_{ab}}}\int_0^\infty d\omega_\beta n_\beta(\omega_\beta)\Bigg\{&\sum_{n_2,n_1\neq b}\frac{-i\omega_{an_1}\langle n_1|\mathbf{e}^*\mathbf{r}|a\rangle}{\omega_{n_1b}} \\ &\times\left[\omega_\beta\langle b|n_2\rangle\langle n_2|n_1\rangle - \omega_\beta\langle b|\mathbf{p}|n_2\rangle\langle n_2|\mathbf{p}|n_1\rangle + \frac{\omega_\beta^3}{3}\langle b|\mathbf{r}|n_2\rangle\langle n_2|\mathbf{r}|n_1\rangle\right]\left(\frac{1}{\omega_{n_2b}+\omega_\beta-i\eta}+\frac{1}{\omega_{n_2b}-\omega_\beta-i\eta}\right) \\ &-\frac{1}{2}\sum_{n_2}(-i\omega_{ab}\langle b|\mathbf{e}^*\mathbf{r}|a\rangle)\left[\omega_\beta\langle b|n_2\rangle\langle n_2|b\rangle - \omega_\beta\langle b|\mathbf{p}|n_2\rangle\langle n_2|\mathbf{p}|b\rangle + \frac{\omega_\beta^3}{3}\langle b|\mathbf{r}|n_2\rangle\langle n_2|\mathbf{r}|b\rangle\right] \\ &\times\left[\frac{1}{(\omega_{n_2b}+\omega_\beta-i\eta)^2}+\frac{1}{(\omega_{n_2b}-\omega_\beta-i\eta)^2}\right]\Bigg\}.\end{aligned} \tag{30}$$

In view of the orthogonality property of wave functions and the inequality $n_1 \neq b$, the term $\omega_\beta\langle b|n_2\rangle\langle n_2|n_1\rangle$ turns to zero. In turn, the term $\omega_\beta\langle b|n_2\rangle\langle n_2|b\rangle$ leads to infrared divergence for $n_2 = b$:

$$\hat{U}_{ab(n_2=b)}^{(3)\text{Fig.2}} = -\frac{e^3}{2\pi^{5/2}}\sqrt{\frac{\omega_{ab}}{2}}\int_0^\infty\frac{d\omega_\beta}{\omega_\beta}n_\beta(\omega_\beta). \tag{31}$$

Below we will show that the same divergences occur for the diagrams in Figs. 3 and 4. In particular, from the combination of these three graphs will follow that the singular contribution for the diagram in Fig. 4 is canceled precisely by the corresponding terms in the diagrams in Figs. 2 and 3. The same is true for the ordinary radiative QED corrections to one-photon transition rates; see [47]. Thus, all the infrared divergences contained in Figs. 2–4 are canceled, removing the terms $\omega_\beta\langle b|n_2\rangle\langle n_2|n_1\rangle$ and $\omega_\beta\langle b|n_2\rangle\langle n_2|b\rangle$ in Eq. (30). Then, Eq. (30) reduces to

$$\begin{aligned}\hat{U}_{ab}^{(3)\text{Fig.2}} = \frac{(-ie)^3}{4\pi^3}\sqrt{\frac{2\pi}{\omega_{ab}}}\int_0^\infty d\omega_\beta n_\beta(\omega_\beta)\Bigg\{&\sum_{n_2,n_1\neq b}\frac{-i\omega_{an_1}\langle n_1|\mathbf{e}^*\mathbf{r}|a\rangle}{\omega_{n_1b}}\left[-\omega_\beta\langle b|\mathbf{p}|n_2\rangle\langle n_2|\mathbf{p}|n_1\rangle + \frac{\omega_\beta^3}{3}\langle b|\mathbf{r}|n_2\rangle\langle n_2|\mathbf{r}|n_1\rangle\right] \\ &\times\left(\frac{1}{\omega_{n_2b}+\omega_\beta-i\eta}+\frac{1}{\omega_{n_2b}-\omega_\beta-i\eta}\right)-\frac{1}{2}\sum_{n_2}(-i\omega_{ab}\langle b|\mathbf{e}^*\mathbf{r}|a\rangle)\left[-\omega_\beta\langle b|\mathbf{p}|n_2\rangle\langle n_2|\mathbf{p}|b\rangle + \frac{\omega_\beta^3}{3}\langle b|\mathbf{r}|n_2\rangle\langle n_2|\mathbf{r}|b\rangle\right] \\ &\times\left[\frac{1}{(\omega_{n_2b}+\omega_\beta-i\eta)^2}+\frac{1}{(\omega_{n_2b}-\omega_\beta-i\eta)^2}\right]\Bigg\}.\end{aligned} \tag{32}$$

Expression (32) can be rewritten in another way,

$$\begin{aligned}\hat{U}_{ab}^{(3)\text{Fig.2}} = \frac{(-ie)^3}{4\pi^3}\sqrt{\frac{2\pi}{\omega_{ab}}}\int_0^\infty d\omega_\beta n_\beta(\omega_\beta)\Bigg\{&\sum_{n_2,n_1\neq b}\frac{-i\omega_{an_1}\langle n_1|\mathbf{e}^*\mathbf{r}|a\rangle}{\omega_{n_1b}}\left[-\omega_\beta\langle b|\mathbf{p}|n_2\rangle\langle n_2|\mathbf{p}|n_1\rangle + \frac{\omega_\beta^3}{3}\langle b|\mathbf{r}|n_2\rangle\langle n_2|\mathbf{r}|n_1\rangle\right] \\ &\times\left(\frac{1}{\omega_{n_2b}+\omega_\beta-i\eta}+\frac{1}{\omega_{n_2b}-\omega_\beta-i\eta}\right)-\frac{1}{2}\sum_{n_2}(-i\omega_{ab}\langle b|\mathbf{e}^*\mathbf{r}|a\rangle)\frac{\partial}{\partial E_b}\left[-\omega_\beta\langle b|\mathbf{p}|n_2\rangle\langle n_2|\mathbf{p}|b\rangle + \frac{\omega_\beta^3}{3}\langle b|\mathbf{r}|n_2\rangle\langle n_2|\mathbf{r}|b\rangle\right] \\ &\times\left(\frac{1}{\omega_{n_2b}+\omega_\beta-i\eta}+\frac{1}{\omega_{n_2b}-\omega_\beta-i\eta}\right)\Bigg\}.\end{aligned} \tag{33}$$

Then, applying relation (10), we obtain the final expression within the nonrelativistic limit for the diagram in Fig. 2,

$$\hat{U}_{ab}^{(3)\mathrm{Fig.2}} = \frac{(-ie)^3}{4\pi^3}\sqrt{\frac{2\pi}{\omega_{ab}}}\int_0^\infty d\omega_\beta n_\beta(\omega_\beta)\Bigg\{\sum_{n_2,n_1\neq b}\frac{-i\omega_{an_1}\langle n_1|\mathbf{e}^*\mathbf{r}|a\rangle\langle b|\mathbf{r}|n_2\rangle\langle n_2|\mathbf{r}|n_1\rangle}{\omega_{n_1b}}\left(-\omega_\beta\omega_{n_2n_1}\omega_{n_2b}+\frac{\omega_\beta^3}{3}\right)$$
$$\times\left(\frac{1}{\omega_{n_2b}+\omega_\beta-i\eta}+\frac{1}{\omega_{n_2b}-\omega_\beta-i\eta}\right)-\frac{i\omega_{ab}\langle b|\mathbf{e}^*\mathbf{r}|a\rangle}{2}\frac{\partial}{\partial E_b}\sum_{n_2}\langle b|\mathbf{r}|n_2\rangle\langle n_2|\mathbf{r}|b\rangle\left(\frac{4\omega_\beta^3}{3}\frac{\omega_{n_2b}}{\omega_{n_2b}^2-\omega_\beta^2}\right)\Bigg\}. \quad (34)$$

Evaluation of the diagram in Fig. 3 repeats the procedure above [see Eqs. (21)–(34)], with the S-matrix element

$$\hat{S}_{ab}^{(3)\mathrm{Fig.3}} = (-ie)^3\int dx_3dx_2dx_1\overline{\psi}_b(x_3)\gamma_{\mu_3}A^*_{\mu_3}(x_3)S(x_3,x_2)e^{-\eta|t_3|}D^\beta_{\mu_2\mu_1}(x_2,x_1)e^{-\eta|t_2|}\gamma_{\mu_2}S(x_2,x_1)\gamma_{\mu_1}e^{-\eta|t_1|}\psi_a(x_1). \quad (35)$$

Then the transition amplitude can be written as

$$\hat{U}_{ab}^{(3)\mathrm{Fig.3}} = \frac{(-ie)^3}{4\pi^3}\sqrt{\frac{2\pi}{\omega_{ab}}}\int_0^\infty d\omega_\beta n_\beta(\omega_\beta)\Bigg\{\sum_{n_1,n_2\neq a}\frac{-i\omega_{n_2b}\langle b|\mathbf{e}^*\mathbf{r}|n_2\rangle\langle n_2|\mathbf{r}|n_1\rangle\langle n_1|\mathbf{r}|a\rangle}{\omega_{n_2a}}\left(-\omega_\beta\omega_{n_2n_1}\omega_{an_1}+\frac{\omega_\beta^3}{3}\right)$$
$$\times\left(\frac{1}{\omega_{n_1a}+\omega_\beta-i\eta}+\frac{1}{\omega_{n_1a}-\omega_\beta-i\eta}\right)-\frac{i\omega_{ab}\langle b|\mathbf{e}^*\mathbf{r}|a\rangle}{2}\frac{\partial}{\partial E_a}\sum_{n_1}\langle a|\mathbf{r}|n_1\rangle\langle n_1|\mathbf{r}|a\rangle\left(\frac{4\omega_\beta^3}{3}\frac{\omega_{n_1a}}{\omega_{n_1a}^2-\omega_\beta^2}\right)\Bigg\}, \quad (36)$$

where the same infrared divergence as in Eq. (31) arises with $n_1 = a$.

Now we can consider the last diagram given by Fig. 4. The corresponding S-matrix element is

$$\hat{S}_{ab}^{(3)\mathrm{Fig.4}} = (-ie)^3\int dx_3dx_2dx_1\overline{\psi}_b(x_3)S(x_3,x_2)e^{-\eta|t_3|}\gamma_{\mu_3}D^\beta_{\mu_3\mu_1}(x_3,x_1)\gamma_{\mu_2}A^*_{\mu_2}(x_2)\gamma_{\mu_1}e^{-\eta|t_2|}S(x_2,x_1)e^{-\eta|t_1|}\psi_a(x_1), \quad (37)$$

Performing integration over time variables and frequencies in the electron and photon propagators, we arrive at the following expression for the transition amplitude:

$$\hat{U}_{ab}^{(3)\mathrm{Fig.4}} = \frac{(-ie)^3}{4\pi^3}\sqrt{\frac{2\pi}{\omega_{ab}}}\Bigg\{\sum_{n_2n_1}(-i)\omega_{n_1n_2}\langle n_2|\mathbf{e}^*\mathbf{r}|n_1\rangle\int_0^\infty d\omega_\beta n_\beta(\omega_\beta)\Bigg[\omega_\beta\langle b|n_2\rangle\langle n_1|a\rangle$$
$$+\left(-\omega_\beta\omega_{bn_2}\omega_{an_1}+\frac{\omega_\beta^3}{3}\right)\langle b|\mathbf{r}|n_2\rangle\langle n_1|\mathbf{r}|a\rangle\Bigg]$$
$$\times\left[\frac{1}{(\omega_{n_2b}+\omega_\beta-i\eta)(\omega_{n_1a}+\omega_\beta-i\eta)}+\frac{1}{(\omega_{n_2b}-\omega_\beta-i\eta)(\omega_{n_1a}-\omega_\beta-i\eta)}\right]\Bigg\}. \quad (38)$$

The infrared divergence in Eq. (38) appears from the term $\omega\langle b|n_2\rangle\langle n_1|a\rangle$, with $n_1 = a$ and $n_2 = b$. Then the divergent part of the amplitude shown in Fig. 4 congregates to

$$\hat{U}^{(3)\mathrm{Fig.4}}_{ab(n_1=a,n_2=b)} = \frac{e^3}{\pi^{5/2}}\sqrt{\frac{\omega_{ab}}{2}}\int_0^\infty\frac{d\omega_\beta n_\beta(\omega_\beta)}{\omega_\beta}. \quad (39)$$

The result (39) has the opposite sign and is twice as large as Eq. (31), canceling the aggregated contribution given by Eq. (31) for Figs. 2 and 3. Then, Eq. (38) can be written in the form

$$\hat{U}_{ab}^{(3)\mathrm{Fig.4}} = \frac{(-ie)^3}{4\pi^3}\sqrt{\frac{2\pi}{\omega_{ab}}}\Bigg\{\sum_{n_2n_1}(-i)\omega_{n_1n_2}\langle n_2|\mathbf{e}^*\mathbf{r}|n_1\rangle\langle b|\mathbf{r}|n_2\rangle\langle n_1|\mathbf{r}|a\rangle\int_0^\infty d\omega_\beta n_\beta(\omega_\beta)\left(-\omega_\beta\omega_{bn_2}\omega_{an_1}+\frac{\omega_\beta^3}{3}\right)$$
$$\times\left[\frac{1}{(\omega_{n_2b}+\omega_\beta-i\eta)(\omega_{n_1a}+\omega_\beta-i\eta)}+\frac{1}{(\omega_{n_2b}-\omega_\beta-i\eta)(\omega_{n_1a}-\omega_\beta-i\eta)}\right]\Bigg\}. \quad (40)$$

Finally, the thermal radiative corrections corresponding to the diagrams in Fig. 2–4, after the integration over photon directions and summation over polarizations, are given by

$$\Delta W_{ab}^{\mathrm{Fig.2}} = -\frac{4e^4}{3\pi}\frac{1}{2l_a+1}\sum_{m_a m_b}\sum_{n_2 n_1}\left\{\sum_{n_2,n_1\neq b}\frac{\omega_{ab}^2\omega_{an_1}\langle a|\mathbf{r}|b\rangle\langle n_1|\mathbf{r}|a\rangle\langle b|\mathbf{r}|n_2\rangle\langle n_2|\mathbf{r}|n_1\rangle}{\omega_{n_1 b}}\mathcal{P}\int_0^\infty d\omega_\beta n_\beta(\omega_\beta)\left(-\omega_\beta\omega_{n_2 n_1}\omega_{n_2 b}+\frac{\omega_\beta^3}{3}\right)\right.$$
$$\left.\times\left(\frac{2\omega_{n_2 b}}{\omega_{n_2 b}^2-\omega_\beta^2}\right)-\frac{\omega_{ab}^3|\langle a|\mathbf{r}|b\rangle|^2|\langle b|\mathbf{r}|n_2\rangle|^2}{2}\frac{\partial}{\partial E_b}\mathcal{P}\int_0^\infty d\omega_\beta n_\beta(\omega_\beta)\sum_{n_2}\left(\frac{4\omega_\beta^3}{3}\frac{\omega_{n_2 b}}{\omega_{n_2 b}^2-\omega_\beta^2}\right)\right\}, \tag{41}$$

$$\Delta W_{ab}^{\mathrm{Fig.3}} = -\frac{4e^4}{3\pi}\frac{1}{2l_a+1}\sum_{m_a m_b}\sum_{n_2 n_1}\left\{\sum_{n_1,n_2\neq a}\frac{\omega_{ab}^2\omega_{n_2 b}\langle a|\mathbf{r}|b\rangle\langle b|\mathbf{r}|n_2\rangle\langle n_2|\mathbf{r}|n_1\rangle\langle n_1|\mathbf{r}|a\rangle}{\omega_{n_2 a}}\mathcal{P}\int_0^\infty d\omega_\beta n_\beta(\omega_\beta)\right.$$
$$\left.\times\left(-\omega_\beta\omega_{n_2 n_1}\omega_{an_1}+\frac{\omega_\beta^3}{3}\right)\left(\frac{2\omega_{n_1 a}}{\omega_{n_1 a}^2-\omega_\beta^2}\right)-\frac{\omega_{ab}^3|\langle a|\mathbf{r}|b\rangle|^2|\langle a|\mathbf{r}|n_1\rangle|^2}{2}\frac{\partial}{\partial E_a}\mathcal{P}\int_0^\infty d\omega_\beta n_\beta(\omega_\beta)\sum_{n_1}\left(\frac{4\omega_\beta^3}{3}\frac{\omega_{n_1 a}}{\omega_{n_1 a}^2-\omega_\beta^2}\right)\right\}, \tag{42}$$

$$\Delta W_{ab}^{\mathrm{Fig.4}} = -\frac{4e^4}{3\pi}\frac{1}{2l_a+1}\sum_{m_a m_b}\sum_{n_2 n_1}\omega_{ab}^2\omega_{n_1 n_2}\langle a|\mathbf{r}|b\rangle\langle n_2|\mathbf{r}|n_1\rangle\langle b|\mathbf{r}|n_2\rangle\langle n_1|\mathbf{r}|a\rangle\mathcal{P}\int_0^\infty d\omega_\beta n_\beta(\omega_\beta)$$
$$\times\left(-\omega_\beta\omega_{n_2 b}\omega_{n_1 a}+\frac{\omega_\beta^3}{3}\right)\frac{2\left(\omega_\beta^2+\omega_{n_2 b}\omega_{n_1 a}\right)}{\left(\omega_{n_2 b}^2-\omega_\beta^2\right)\left(\omega_{n_1 a}^2-\omega_\beta^2\right)}. \tag{43}$$

Here the principal value of integral, $\mathcal{P}$, has appeared as a result of taking the real part in Eq. (24) and applying the Sokhotski-Plemelj theorem in the limit $\eta \to 0$.

In addition to the thermal QED corrections derived above, we must take into account the contribution originating from changing the photon energy ω_{ab} in the zero-order transition probability given by Eq. (12) due to the BBR-induced Stark shifts of the energies of the bound states a and b. Within the framework of finite-temperature QED of the bound states, the BBR-induced Stark shift corresponds to the thermal one-loop SE diagram; see Fig. 5. Recently, this graph was evaluated in [37], where the real part representing the Stark shift was found to be in complete agreement with the equation obtained in [35] within the quantum mechanical approach. Following [35,37], the Stark shift is given by

$$\Delta E_a^\beta = \frac{1}{2l_a+1}\sum_{m_a m_b}\frac{4e^2}{3\pi}\sum_n|\langle a|\mathbf{r}|n\rangle|^2\mathcal{P}\int_0^\infty d\omega_\beta\omega_\beta^3 n_\beta(\omega_\beta)$$
$$\times\frac{\omega_{an}}{\omega_{an}^2-\omega_\beta^2}. \tag{44}$$

Numerical values of ΔE_a^β at different temperatures are collected in Table I for the $1s$, $2s$, and $2p$ states in the hydrogen atom. The BBR-induced Stark shifts for states a and b, related to the real part of the diagram in Fig. 5, also contribute to the photon energy ω_{ab} and, consequently, to the transition rate. The corresponding correction can be written as a difference between the transition rate given by Eq. (12) calculated with zero-order photon energy ω_{ab} and the Stark-shift corrected

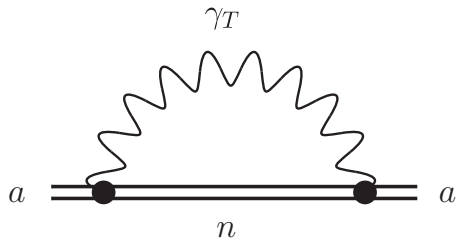

FIG. 5. The Feynman graph corresponding to the thermal one-loop electron self-energy. The wavy line with index γ_T denotes the thermal photon propagator. The real part of this graph corresponds to the thermal Stark shift, while the imaginary part represents the induced one-photon width Γ_a^{BBR} of the atomic energy level a.

TABLE I. Blackbody-radiation-induced dynamic Stark shifts (Hz) of energy levels of hydrogen at different temperatures (Kelvin). The numbers in square brackets indicate powers of ten. Fine structure and the Lamb shift were neglected in performing the calculation. The asterisks correspond to the values presented in [35].

T	$1s$	$2s$	$2p$
300	−3.8754[−2]	−1.0434	−1.5181
	−4.128[−2]*	−1.077*	−1. 535*
1000	−4.7893	−1.3229[2]	−1.9438[2]
3000	−3.9148[2]	−1.4111[4]	−2.1033[4]
5000	−3.0797[2]	−7.6499[4]	−1.0774[5]
8000	−2.1370[4]	−1.2917[5]	−1.2786[5]
10000	−5.5601[4]	−3.0019[4]	9.3418[4]
50000	−2.5583[6]	4.5616[7]	6.0049[7]

TABLE II. Corrections to one-photon transition rates corresponding to Figs. 2–4, induced transition rates $W_{2p1s}^{\rm ind}$, and BBR-induced width $\Gamma_{2p}^{\rm BBR}$ in s^{-1} at different temperatures (Kelvin). The numbers in the square brackets indicate powers of ten. All calculations were performed in the Feynman gauge of the thermal photon propagator.

T	$\Delta W_{2p1s}^{\rm Fig.2}$	$\Delta W_{2p1s}^{\rm Fig.3}$	$\Delta W_{2p1s}^{\rm Fig.4}$	$\Delta W_{2p1s}^{\rm Stark}$	$\Delta W_{2p1s}^{\rm total}$	$W_{2p1s}^{\rm ind}$	$\Gamma_{2p}^{\rm BBR}$
300	−6.3948[−5]	1.5111[−3]	9.7273[−4]	1.1547[−6]	2.4210[−3]	2.3598[−163]	4.7430[−6]
1000	−7.1011[−4]	1.7011[−2]	1.0883[−2]	1.4450[−4]	2.7328[−2]	2.3435[−43]	3.2943[−2]
3000	−6.3567[−3]	1.7575[−1]	1.0602[−1]	1.5731[−2]	2.9114[−1]	4.5156[−9]	7.5856[4]
5000	−1.7445[−2]	4.1682[−1]	3.1890[−1]	7.9768[−2]	7.9804[−1]	3.2486[−2]	1.5306[6]
8000	−4.0087[−2]	6.6053[−1]	7.83286[−1]	8.1160[−2]	1.4849	2.3373[2]	9.2948[6]
10000	−6.3120[−2]	8.4717[−1]	1.1223	−1.1357[−1]	3.3473[−1]	4.5126[3]	1.7960[7]
50000	−5.1929	2.8715[1]	−3.7875	−4.7716[1]	−2.79814[1]	6.4759[7]	4.4084[8]

photon energy $\tilde{\omega}_{ab} = E_a + \Delta E_a^{\beta} - E_b - \Delta E_b^{\beta}$ [47],

$$\Delta W_{ab}^{\rm Stark} = \frac{1}{2l_a+1}\sum_{m_a m_b}\frac{4e^2}{3}\left(\omega_{ab}^3 - \tilde{\omega}_{ab}^3\right)|\langle b|\mathbf{r}|a\rangle|^2. \quad (45)$$

Finally, the total thermal QED correction, arising from the graphs in Figs. 2–5, to the one-photon transition rate is given by

$$\Delta W_{ab}^{\rm total} = \Delta W_{ab}^{\rm Fig.2} + \Delta W_{ab}^{\rm Fig.3} + \Delta W_{ab}^{\rm Fig.4} + \Delta W_{ab}^{\rm Stark}. \quad (46)$$

Here, $\Delta W_{ab}^{\rm Fig.2}$, $\Delta W_{ab}^{\rm Fig.3}$, $\Delta W_{ab}^{\rm Fig.4}$, and $\Delta W_{ab}^{\rm Stark}$ are defined by Eqs. (41)–(43) and (45), respectively. These corrections were obtained in the nonrelativistic limit as the contributions of leading order in α. Numerical values of $\Delta W_{ab}^{\rm Fig.2}$, $\Delta W_{ab}^{\rm Fig.3}$, $\Delta W_{ab}^{\rm Fig.4}$, and $\Delta W_{ab}^{\rm Stark}$ for the $2p \to 1s + \gamma$(E1) transition in the hydrogen atom at different temperatures are collected in Table II. All calculations were performed in the Feynman gauge of the thermal photon propagator. It is important to note that the diagrams depicted in Figs. 2–4 are physically inseparable and only their total contribution is gauge invariant and makes physical sense.

IV. CONCLUSIONS AND DISCUSSION

In this work, the thermal one-loop self-energy corrections to the one-photon transition rate were obtained within the framework of QED theory. The partial transition probabilities and total depopulation rates induced by the BBR field [see Eqs. (12) and (13)] at different temperatures were also evaluated. The numerical values are given in Table II. For the summation over the entire spectrum in Eqs. (41)–(43), the B-spline method was employed [48]. The spectrum of virtual states was checked on calculation of Stark shifts and depopulation rates; see Tables I and II. As an additional verification, the Thomas-Reiche-Kuhn sum rule was also checked by this method. The results of the calculations for BBR-induced Stark shifts at $T = 300$ K are in excellent agreement with our previous results [37]. However, at high temperatures, the present calculations are more accurate due to the improved numerical integration over ω_β in Eq. (44).

As an example, we focused on the numerical evaluation of Eq. (46) for the Ly$_\alpha$ $2p \to 1s + \gamma$(E1) transition in hydrogen atom; see Table II. To demonstrate the role of thermal QED corrections, it is useful to compare them with the "ordinary" QED corrections. The radiative QED correction of lowest order to the Ly$_\alpha$ transition was found in [3] as

$$\Delta W_{2p1s}^{\rm QED} = W_{2p1s}\frac{\alpha}{\pi}(\alpha Z)^2\left[\left(\frac{8}{3}\ln\frac{4}{3} - \frac{61}{18}\right)\ln(\alpha Z)^{-2} + 6.57603\right] \approx -1490\ {\rm s}^{-1}, \quad (47)$$

where $W_{2p1s} = 6.268 \times 10^8$ s^{-1} is the spontaneous one-photon decay rate of the lowest order; see Eq. (11). As seen in Table II, the thermal radiative SE corrections contribute to the ordinary QED correction $\Delta W_{2p1s}^{\rm QED}$ at a level of several percent and more, beginning from temperatures greater than 50 000 K.

The fundamental importance of the theoretical value of the Ly$_\alpha$ transition rate W_{2p1s} in neutral hydrogen is caused by determining the $2p - 2s$ Lamb shift. For a successful comparison of theory and experimental measurements, it is necessary to know the theoretical rate of the $2p \to 1s + \gamma$(E1) transition with a precision of 10^{-6}–10^{-8} [49,50]. Assuming that the experiment is carried out at room temperature $T = 300$ K, the thermal radiative QED correction found in the present work is of the relative magnitude 10^{-11}. This is, however, several orders less than the current accuracy of the Lamb shift determination, but could be important for future precise measurements.

It can also be expected that thermal corrections considered in the present work could play a role in various astrophysical applications when the radiative processes are considered at higher temperatures. In particular, the theoretical and experimental analysis of line intensities of quasars and similar objects where the radiation temperature reaches several tens of thousands of degrees requires the knowledge of atomic transition rates and level populations [51–53]. It is worth noting that the Lyman alpha line, as well as the 21 cm line, is the main source of identification of distant quasars [54]. Concerning this, it is more correct to analyze thermal radiative QED corrections with respect to the BBR-induced transition rates, which plays an important role in rate equations of population balance [26]. From Eqs. (41)–(43), it follows that the parametric estimation of the leading order in α for the thermal contributions $\Delta W_{ab}^{\rm Fig.2}$, $\Delta W_{ab}^{\rm Fig.3}$, and $\Delta W_{ab}^{\rm Fig.4}$ is the same as the simplest correction arising via the Stark shift, given by Eq. (45). Then the magnitudes of $\Delta W_{ab}^{\rm Fig.2}$, $\Delta W_{ab}^{\rm Fig.3}$, and $\Delta W_{ab}^{\rm Fig.4}$ at room temperature are about a hundred times larger than the induced transition rate, $W_{2p1s}^{\rm ind}$. They become

comparable at the temperatures about $T = 6000$–8000 K. Beginning from 8000 K, the thermal radiative corrections become less than the BBR-induced transition rate $W^{\rm ind}_{2p1s}$. From Table II, it also follows that the BBR-induced line broadening $\Gamma^{\rm BBR}_{2p}$ is the same order of magnitude as the corrections in Eq. (46) at the temperature $T = 1000$ K and exceeds $\Delta W^{\rm total}_{2p1s}$ at higher temperatures. The results are applicable up to the hydrogen ionization temperature $T_{\rm ion} \sim 157\,000$ K, when corrections Eqs. (41)–(43) and (45) may be even more important than the radiative QED effects given by Eq. (47). In conclusion, a different type of radiative and temperature dependent corrections to the decay rates was introduced. Despite the relative smallness of these corrections, they may be important in certain laboratory experiments and astrophysical problems dealing with the BBR-induced effects.

ACKNOWLEDGMENTS

The work of T. Z. was supported by the Foundation for the Advancement of Theoretical Physics and Mathematics "BASIS." The work was also supported by RFBR Grant No. 20-02-00111.

[1] G. W. F. Drake, Phys. Rev. A **9**, 2799 (1974).
[2] J. Sucher, Phys. Rev. **107**, 1448 (1957).
[3] J. Sapirstein, K. Pachucki, and K. T. Cheng, Phys. Rev. A **69**, 022113 (2004).
[4] A. V. Volotka, D. A. Glazov, G. Plunien, V. M. Shabaev, and I. I. Tupitsyn, Eur. Phys. J. D **38**, 293 (2006).
[5] T. V. Back, H. S. Margolis, P. K. Oxley, J. D. Silver, and E. G. Myers, Hyperfine Int. **114**, 203 (1998).
[6] D. P. Moehs and D. A. Church, Phys. Rev. A **58**, 1111 (1998).
[7] E. Träbert, G. Gwinner, A. Wolf, X. Tordoir, and A. G. Calamai, Phys. Lett. A **264**, 311 (1999).
[8] E. Träbert, P. Beiersdorfer, S. B. Utter, G. V. Brown, H. Chen, C. L. Harris, P. A. Neill, D. W. Savin, and A. J. Smith, Astrophys. J. **541**, 506 (2000).
[9] E. Träbert, P. Beiersdorfer, G. V. Brown, H. Chen, E. H. Pinnington, and D. B. Thorn, Phys. Rev. A **64**, 034501 (2001).
[10] E. Träbert, P. Beiersdorfer, G. Gwinner, E. H. Pinnington, and A. Wolf, Phys. Rev. A **66**, 052507 (2002).
[11] J. R. Crespo Lopez-Urrutia, A. N. Artemyev, J. Braun, G. Brenner, H. Bruhns, I. N. Draganic, A. J. Gonzalez Martinez, A. Lapierre, V. Mironov, J. Scofield, R. Soria Orts, H. Tawara, M. Trinczek, I. I. Tupitsyn, and J. Ullrich, Nucl. Instr. Meth. Phys. Res. B **235**, 85 (2005).
[12] A. Lapierre, U. D. Jentschura, J. R. Crespo Loópez-Urrutia, J. Braun, G. Brenner, H. Bruhns, D. Fischer, A. J. Gonzalez Martínez, Z. Harman, W. R. Johnson, C. H. Keitel, V. Mironov, C. J. Osborne, G. Sikler, R. Soria Orts, V. Shavaev, H. Tawara, I. I. Tupitsyn, J. Ullrich, and A. Volotka, Phys. Rev. Lett. **95**, 183001 (2005).
[13] Z. Fried and A. O. Martin, Nuovo Cim. **29**, 574 (1963).
[14] G. S. Adkins and J. Sapirstein, Phys. Rev. A **78**, 062503 (2008).
[15] S. G. Karshenboim, Phys. Rev. A **56**, 4311 (1997).
[16] I. I. Tupitsyn, A. V. Volotka, D. A. Glazov, V. M. Shabaev, G. Plunien, J. R. Crespo Lopez-Urrutia, A. Lapierre, and J. Ullrich, Phys. Rev. A **72**, 062503 (2005).
[17] G. W. F. Drake, Phys. Rev. A **5**, 1979 (1972).
[18] H. F. Beyer and V. P. Shevelko, *Introduction to the Physics of Highly Charged Ions* (Institute of Physics, Bristol, 2003).
[19] J. Sapirstein, K. Pachucki, A. Veitia, and K. T. Cheng, Phys. Rev. A **67**, 052110 (2003).
[20] V. M. Shabaev, I. I. Tupitsyn, K. Pachucki, G. Plunien, and V. A. Yerokhin, Phys. Rev. A **72**, 062105 (2005).
[21] T. Zalialiutdinov, D. Solovyev, L. Labzowsky, and G. Plunien, Phys. Rev. A **89**, 052502 (2014).
[22] B. J. Wundt and U. D. Jentschura, Phys. Rev. A **80**, 022505 (2009).
[23] F. Riehle, *Frequency Standards: Basics and Applications* (Wiley-VCH Verlag GmbH & Co. KGaA, Weinheim, 2004).
[24] L. N. Labzowsky, G. L. Klimchitskaya, and Yu. Dmitriev, *Relativistic Effects in the Spectra of Atomic Systems* (IOP, Bristol, 1993).
[25] E. S. Fradkin, D. M. Guitman, and S. M. Shvartsman, *Quantum Electrodynamics with Unstable Vacuum* (Springer-Verlag, Berlin, 1991).
[26] S. A. Kaplan and S. B. Pikelner, *The Interstellar Medium* (Harvard University Press, Cambridge, 1970).
[27] D. Solovyev, V. Sharipov, L. Labzowsky, and G. Plunien, J. Phys. B: At. Mol. Opt. Phys. **43**, 074005 (2010).
[28] K. W. Martin, B. Stuhl, J. Eugenio, M. S. Safronova, G. Phelps, J. H. Burke, and N. D. Lemke, Phys. Rev. A **100**, 023417 (2019).
[29] T. Middelmann, S. Falke, C. Lisdat, and U. Sterr, Phys. Rev. Lett. **109**, 263004 (2012).
[30] M. S. Safronova, S. G. Porsev, U. I. Safronova, M. G. Kozlov, and C. W. Clark, Phys. Rev. A **87**, 012509 (2013).
[31] I. I. Beterov, D. B. Tretyakov, I. I. Ryabtsev, V. M. Entin, A. Ekers, and N. N. Bezuglov, New J. Phys. **11**, 013052 (2009).
[32] V. D. Ovsiannikov, I. L. Glukhov, and E. A. Nekipelov, J. Phys. B: At. Mol. Opt. Phys. **44**, 195010 (2011).
[33] J. Chluba and R. A. Sunyaev, Astron. Astrophys. **446**, 39 (2006).
[34] C. M. Hirata, Phys. Rev. D **78**, 023001 (2008).
[35] J. W. Farley and W. H. Wing, Phys. Rev. A **23**, 2397 (1981).
[36] D. Solovyev, Ann. Phys. **415**, 168128 (2020).
[37] D. Solovyev, L. Labzowsky, and G. Plunien, Phys. Rev. A **92**, 022508 (2015).
[38] T. Zalialiutdinov, D. Solovyev, and L. Labzowsky, J. Phys. B: At. Mol. Opt. Phys. **51**, 015003 (2018).
[39] T. Zalialiutdinov, D. Solovyev, L. Labzowsky, and G. Plunien, Phys. Rev. A **96**, 012512 (2017).
[40] D. Solovyev, T. Zalialiutdinov, A. Anikin, J. Triaskin, and L. Labzowsky, Phys. Rev. A **100**, 012506 (2019).
[41] F. Low, Phys. Rev. **88**, 53 (1952).
[42] O. Yu. Andreev, L. N. Labzowsky, G. Plunien, and D. A. Solovyev, Phys. Rep. **455**, 135 (2008).
[43] T. A. Zalialiutdinov, D. A. Solovyev, L. N. Labzowsky, and G. Plunien, Phys. Rep. **737**, 1 (2018).
[44] L. Labzowsky, V. Karasiev, I. Lindgren, H. Persson, and S. Salomonson, Phys. Scripta **T46**, 150 (1993).

[45] L. Labzowsky, D. Solovyev, and G. Plunien, Phys. Rev. A **80**, 062514 (2009).
[46] A. I. Akhiezer and V. B. Berestetskii, *Quantum Electrodynamics* (Wiley, New York, 1965).
[47] V. M. Shabaev, Phys. Rep. **356**, 119 (2002).
[48] V. M. Shabaev, I. I. Tupitsyn, V. A. Yerokhin, G. Plunien, and G. Soff, Phys. Rev. Lett. **93**, 130405 (2004).
[49] S. G. Karshenboim, Phys. Rep. **422**, 1 (2005).
[50] V. G. Palchikov, Y. L. Sokolov, and V. P. Yakovlev, Phys. Scripta **55**, 33 (1997).
[51] K. Davidson and H. Netzer, Rev. Mod. Phys. **51**, 715 (1979).
[52] Y. Y. Kovalev *et al.*, Astrophys. J. Lett. **820**, L9 (2016).
[53] V. Dubrovich, S. Grachev, and T. Zalialiutdinov, Astron. Astrophys. **619**, A29 (2018).
[54] E. Banados *et al.*, Nature (London) **553**, 473 (2018).